Underwater Wireless Power Transfer for Ocean System Applications

Tyler M. Hayslett, Taofeek Orekan, *Student Member, IEEE*, Peng Zhang, *Senior Member, IEEE*

Abstract— The field of wireless power transfer (WPT) has been revitalized since the development of resonant induction technique. Recent research has covered new areas for WPT system in air. However, for WPT in the ocean environment, it is still very much in the research portion of its development. The stochastic nature of the ocean makes transferring power wirelessly very difficult to achieve. This paper investigates and overcomes some of the difficulties that wireless power transfer faces in a salt water environment. The results show that proper coil winding and the addition of resonator circuits increase transmission efficiency. Since the properties of the coils contribute to the efficiency of the WPT system, a detailed study of the system is analyzed to determine the self-inductance, capacitance, parasitic resistance, and the best coil shape.

Index Terms— Power Electronics, Ocean System, Underwater Wireless Power, Coil Design, RLC Circuit.

I. INTRODUCTION

THE ability to transfer power wirelessly allows interconnected system components to eliminate costly wires and connectors. The implementation is particularly advantageous to distributed ocean systems, such as autonomous underwater vehicle (AUV), unmanned surface vehicles (USV), acoustic modems, underwater sensing nodes, ocean censors and monitoring technology, etc. These devices have poor battery life, and consume excessive power which cannot be easily replace by existing power system. The high maintenance and replacement costs of batteries cannot offer sustainable operation. Also, the already burdensome tasks of carrying, operating, and maintaining multiple batteries will only be exacerbated.

Prior research has investigated the use of underwater docking system platform to recharge AUV batteries [1], which are often range-limited by their battery, and rely on manual replacement techniques. The drawback in this method is that it is limited to one specific type of AUV, a larger or small diameter hull AUV will not fit into the docking system. Also, once electrical contacts are exposed to seawater there is a possibility of shorting and corrosion.

Wireless power transfer could eliminate the need for expensive cabling and fault prone electrical connectors currently in use in marine systems.

The primary motivation for exploring underwater WPT (UWPT) is to eliminate the need to replace submerged devices that have short battery life. UWPT provides a method of powering these devices wirelessly, reducing the cost to replace the batteries, increasing reliability and sustainability. The goal is to allow autonomous underwater vehicles to recharge at or near wave energy conversion (WEC) buoys [2]. This would reduce the need for active personnel and boats to service AUVs, extending operational life-cycle and reducing overhead.

Wireless power transfer can be accomplished through acoustic signals [3]. The sound waves or acoustic signal are created by a “transducer” which is a technical term for an underwater antenna. The transducer converts electrical energy into mechanical energy (vibrations) which in turn creates the sound waves. Since transducers and other marine sound equipment require high precision mechanical design and involve high unit costs, there is little interest in using this method. Another method is using beamed power [4]. Using microwaves, lasers, and other forms of EM generation [5], focused power can be delivered over immense distances. In fact, there has been serious discussion of powering space based equipment with various types of beamed power. Unfortunately, studies as far back as the 60's has shown that transmitted EM signals attenuate incredibly quickly in the ocean.

In this paper, resonant wireless power transfer method is explored for powering underwater devices [6] [7]. Resonant wireless power transfer operates under much the same principle as inductive coupling, that is, energy is exchanged through an oscillating magnetic field [8]. The difference lies in the coils. Where inductive coupling only uses two coils (Primary and Secondary sides), resonant transfer utilizes four coils. In inductive coupling, if the primary coil doesn’t transfer the energy away it is just pumped back into the source. In resonant transfer, there are two middle coils that are electrically isolated. Each an RLC circuit, they are tuned to the same resonant frequency. The primary, or the drive coil, transfers energy to the closer resonant coil. Since there is a lack of source, all energy not captured by the third coil is simply recycled into the capacitor, cycles back and resonate. Hence, system power losses are mainly due to the resonant coil resistance.

II. SYSTEM STRUCTURE

Fig. 1 shows the UWPT system. The system consists of four coil resonant circuits, linked by coupling coefficients M_{12}, M_{13}, M_{14}, M_{23}, M_{34}. The transmitting coil (Tx) consists of the

The authors are with the Department of Electrical and Computer Engineering, University of Connecticut, Storrs, CT 06269 USA (e-mail: taofeek.orekan@uconn.edu).

978-1-5090-1537-5/16/$31.00 ©2016 IEEE

capacitor (C_1), to make the drive loop resonant at the intended frequency, and the self-capacitance C_2. R_1 and R_2 represents the parasitic resistance of Tx, and the inductors L_1 and L_2 are magnetically coupled via the coupling coefficient M_{12}; The receiving coil (Rx) is characterized similarly.

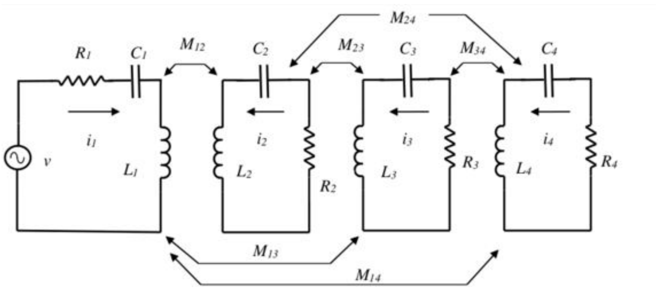

Fig. 1. Full circuit representation of RWPT system

To generate the resonant coupling, a series of LC-connected coils with the same resonant frequency is required. The resonant frequency of each coil was determined by

$$f = \frac{1}{2\pi\sqrt{LC}} \tag{1}$$

$$k_{xy} = \frac{M_{xy}}{\sqrt{L_x L_y}}, \qquad 0 \le k_{xy} \le 1 \tag{2}$$

In equation 2, the coupling coefficient M_{23} represents the mutual inductance that links via a magnetic field the transmitting and receiving coils. Fig. 2 shows the power flow diagram of the four-coil wireless power transfer system.

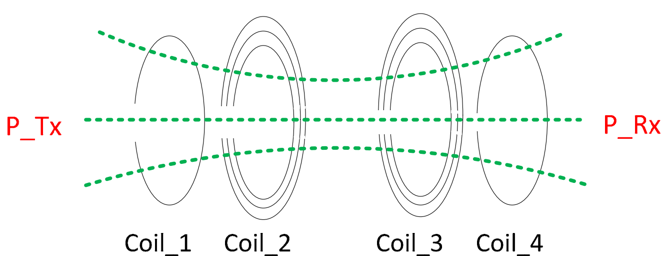

Fig. 2. Power Flow Diagram

The coil_1,2,3,4 represent the power driving coil, sending resonator, receiving resonator and load coil. Each coil will cause some losses which can be represented by a parasitic resistor. The system power balance equation is:

$$P_{Tx} = P_{r1} + P_{r2} + P_{r3} + P_{r4} + P_{Rx} \tag{3}$$

And the power transfer efficiency is calculated as;

$$\eta = \frac{P_{Rx}}{P_{Tx}} = \frac{P_{Rx}}{P_{r1} + P_{r2} + P_{r3} + P_{r4} + P_{Rx}} \tag{4}$$

III. System Analysis and Preliminary Testing

In the preliminary testing, two experiments were performed. They quantified, respectively, the advantaged of a 4 coil resonant system and the attenuation response salt water had to frequency increases for resonant UWPT

A. Test coil design

Initial testing was performed with helical coils as they are the easiest to build. The assumption made was that later improvements in coil design would only effect the slope or rate of attenuation, but not the general trends associated with frequency changes and distance. Complex coil construction and modeling was unnecessary for preliminary testing.

The coils were wound on 3 inches PVC pipe that had been turned down to half thickness. With 35 turns per coil, they had an individual inductance of 607.9μH. Each piece of PVC had two coils, one to act as driver/receiver and a second to serve as a resonator. Fig. 3 shows the preliminary test setup. The coils were insulated (completely sealed off) from the salt water with RTV gasket sealer. Connector wires were attached and sealed to the PVC body. Each coil could then be connected individually to external testing circuitry.

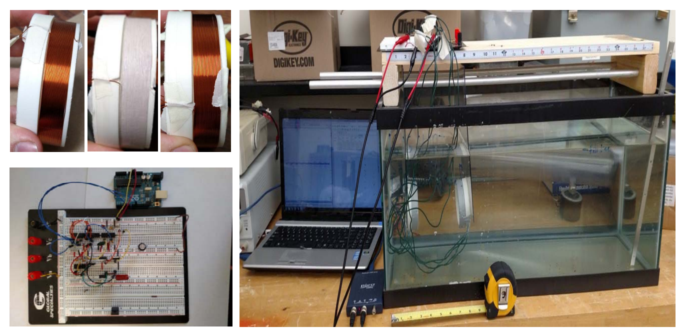

Fig. 3. Preliminary Test setup

B. Test Environment

All submerged tests for the project were done in a 20gallon fish tank. The water was simple tap water, left to sit so the fluoride could evaporate. 50 liters of water and 1.815kg of salt were added to bring the solution to 3.63% salt. Ocean water is between 3.5-4.1% salt, so the solution accurately models a marine environment with the added benefit of not containing marine life.

C. Test procedure

There were two tests carried out, each had its own procedure. Both tests used a signal generator to produce a 50mV amplitude sine wave for V_{source}. The output voltage was measured over C_4. For all measurements, the coils were re-tuned to resonance. This was done by adjusting the frequency until the input and output waves were maximized and in phase. This was important to control as resonant frequency changed with both the immersion in water and the change in distance.

The second test was conducted in a similar manner. For three capacitance values (.1μF, .01μF, and .001μF) the distance sweep was performed in air. The sweeps were then repeated in water for 6 total sweeps. C_2 and C_3 were included in all sweeps for the second test.

D. Test Results

The two tests were compared for a range of frequencies and distances, to show the UWPT system in salt water, and how the addition of intermediary resonant circuits affected received power. The results are shown in Fig. 4, 5, and 6. In Fig. 4, the system with a resonant circuit, that is, the removal of C_2 and C_3 decreased received signal by about 1.75dB at 19.5kHz. Fig. 5 and 6 shows the comparison of the WPT in air and water. The increase in resonant frequency improved received signal while the system operated in air. However, while submerged in water, increases in frequency reduced received signal. At 20kHz(0.1μF), the curves in air and in water were quite similar.

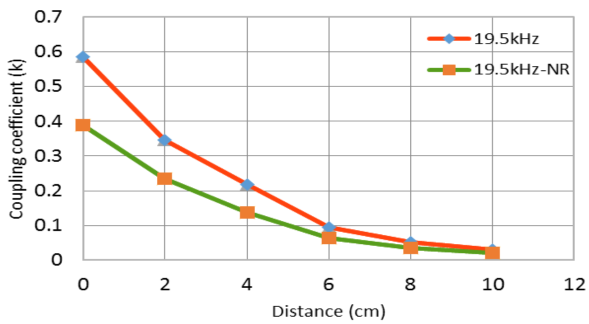

Fig. 4. Distance vs. attenuation for a system with and without two intermediary resonators

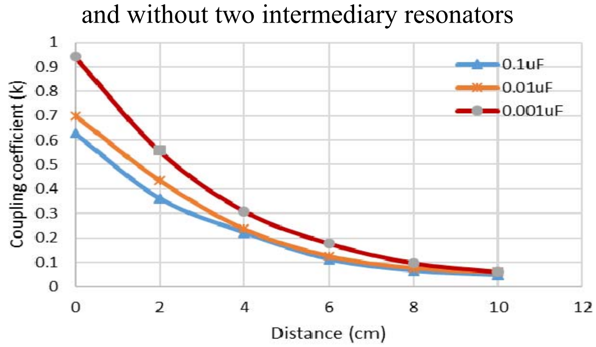

Fig. 5. Distance vs. attenuation for 3 values of capacitor in air

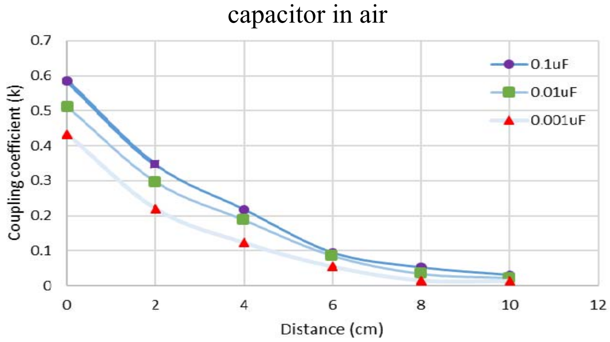

Fig. 6. Distance vs. attenuation for 3 values of capacitor in water

IV. Whole UWPT System Design and Simulations

A. System Requirements

The implemented system consists of a frequency controller, an inverter, the transmitting and receiving coils, and the rectifier with a dummy load attached. The transfer system draws power from the wave energy converter it is mounted on, and captured power in 13.8V lead acid batteries. This is therefore the supply voltage for the UWPT system.

The system is required to be reasonable size. While increasing coil diameter increases can improve transfer efficiency, the Rx coil has to fit on a AUV, which tends to be compact devices. An upper limit of 100mm was chosen for coil diameter.

The preliminary testing observations and results gave two obvious guidelines for the whole system design. The first was the case that the inclusion of the intermediary coils improved transfer efficiency dramatically. The second was that the similarity between the trend lines for 20kHz (0.1μF) in both air and water indicate maximum efficiency. Lower frequencies would decrease coupling in either medium, and higher frequencies would increase losses in the water. While improved coil design would likely change system frequency response, the maximum would likely still be in the low kHz.

Lastly, the whole system needs to be inexpensive and relatively high power. AUV battery capacity is usually in excess of 1.2kWh. Charging at too slow a rate could potentially leave the AUV expending more energy staying in range of the WEC buoy than it is receiving, and lengthy charging times reduce effective operating time for the AUV.

B. Power Electronics System

The inverter is a basic power MOSFET h-bridge circuit shown in Fig. 7. It provides up to 27.6V square waves over the coils depending on battery charge. Because of the high switching speeds and back EMF, MOSFET and driver selection had to be fairly distinct. The high switching speeds meant that large peak currents had to be provided to the MOSFET gate. Since the chosen MOSFETs had small gate charges, the total energy expended is small. It just had to be done very quickly (<100ns). Hence, high current MOSFET drivers were chosen and with quite a margin of safety. The back EMF the coil would generate at resonance meant that the MOSFETs had to have high speed clamping diodes and reverse bias voltages. Peak gate current is calculated using equation 5.

$$I_{Peak} = C \cdot \frac{dV}{dt} = \frac{q}{dt} \cdot \frac{dV}{dt} \tag{5}$$

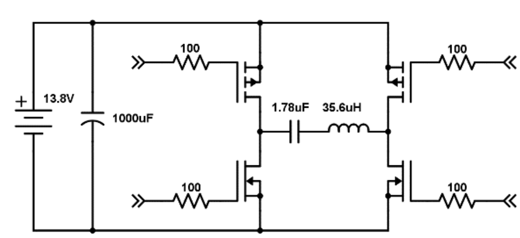

Fig. 7. H-Bridge schematic

The only way to verify the system is actually transferring power is to load it. Since AC loads get "complex", DC loading makes calculations much simpler. The full system would involve a rectifier and some sort of buck-boost to charge the

AUV batteries. The batteries and buck-boost were replaced with a pure resistive load. Shown in Fig. 8, is the assembled rectifier in the receiving side of the UWPT system. High speed, low V_D Schottky diodes (0.251V) form a full wave rectifier with a 3300uF smoothing capacitor. The rectifier is rated to 20A and 60V, well in excess of currently transmitted power. The five 10Ω resistors allow for varied load combinations.

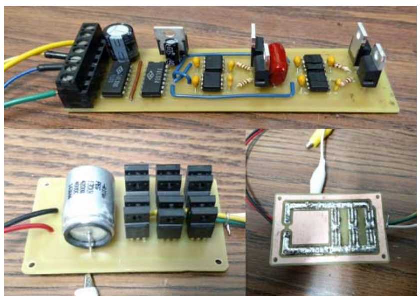

Fig. 8. Assembled Power Electronics

Both the rectifier and the H-bridge were finalized with custom PCBs. Permanent component attachment cleaned up appearances and improved safety. The PCBs were made using a toner masking technique. The board was designed on EagleCAD and printed on high gloss magazine paper. It was later ironed onto a copper clad fiber board. The toner adhered to the copper, and the paper was soaked off with hot water. The board was then placed in a bath of ferric acid to dissolve the exposed copper. The traces could then be exposed, using nail polish remover to clear away the toner. Lastly, the board was drilled and populated

C. Power Electronics Control

The control for the inverter consisted of an ATmega328P on an Arduino Uno shield. This provided an easy platform for debugging and the possibility of adding more complex control algorithms. The ATmega328P has 3 PWM outputs. Two of the PWM signals were routed through 5V logic to provide the 4 switching signals.

Safe h-bridge operation requires that only one direction is on at a time and that there is a dead zone in between to allow for the FETs to fully turn off. This avoids "shoot through", where two FETs on one side are both on, creating a dead short. The ATmega328P generates its PWM signals from on-board counters. Two are 8-bit precision, and one is 16-bit. One of the 8-bit counters was used to provide a square wave at the desired frequency. When the wave is high, one pair of FETs is conducting, when it is low the other pair conducts. The 16-bit PWM signal is high for all but a short low period. This low period is the "dead zone", where none of the MOSFETs are On.

The ATmega328P chip is programed through the Arduino AVRdude interface with ATMEL Studio. This allows low level C control of board functions and register writing. The arduino currently produces a 20kHz switching frequency, the resonance for the chosen capacitor and coils with no separation

D. Coil Analysis and Design

In order to build a wireless power transfer system that would work efficiently underwater, proper description of its behavior is necessary. Coil design involving intensive simulation is required. With the goal of optimizing transmission efficiency, ANSYS Maxwell was used to preform magnetostatic computation of coil coupling factor over a range of coil variables. The simulations exhaustively covered changes in distance, wire thickness, wire separation, coil shape, number of turns, and diameter.

The coupling coefficient is the best metric for coil design. It is the measure of how much of the Tx coils flux is captured by the Rx coil. Fig. 9 shows the magnetic field visualization of the WPT in underwater environment. The larger the percentage captured, the higher maximum system efficiency can be. The results in Fig. 10 shows that the coupling coefficient increased with area and number of turns. The result also demonstrate that Coil shape has a dramatic effect on coupling. The general optimum shape is a high turn coil with thick gauge wire in a flat spiral as large as possible.

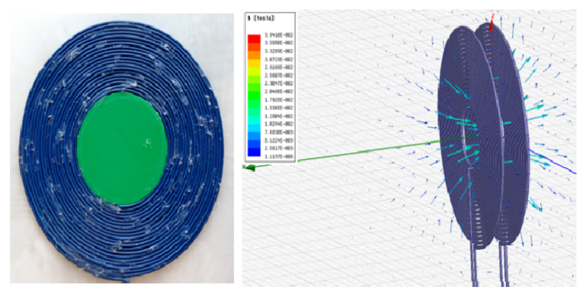

Fig. 9. B-field visualization for 18 turn coil

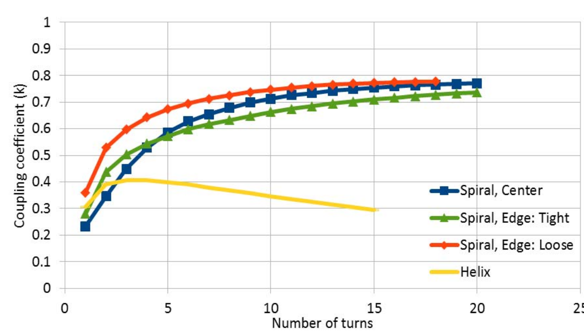

Fig. 10. Coupling factor vs. number of turns for different coil shapes

The final coil for this project was chosen to be a spiral 100mm 20 turn coil, constructed from 20ga wire. Fig. 11 shows the simulation result of the coupling coefficient over a distance of 150 cm. The optimal wire spacing/pitch was found to be 1.45mm (wire center to wire center). Since positioning each turn free-hand proved incredibly complicated, wire with an insulation thickness of 0.25mm was chosen. This allowed for a pitch of ~1.35mm with the winding insulation touching.

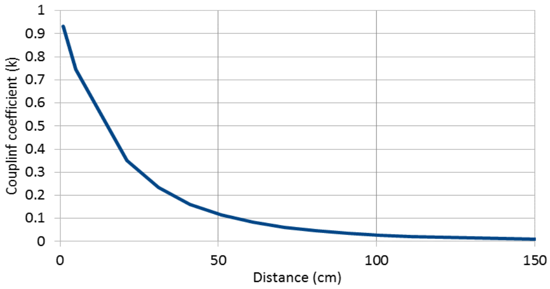

Fig. 11. Whole System Coupling vs. Distance

The coil has an inductance of 35.6uH, and was mounted on Lexan to allow for immersed testing. This provided the inner diameter spacing calculated in Maxwell, and allowed the coils to completely concentric to each-other in the test stand.

V. Experimental Results

A. Subsystem Testing

Component testing was fairly rapid. The switching signals were tested on a breadboard, followed by inverter assembly and demonstration. Fig. 12 and 13 shows the inverter output and the full h-bridge output results.

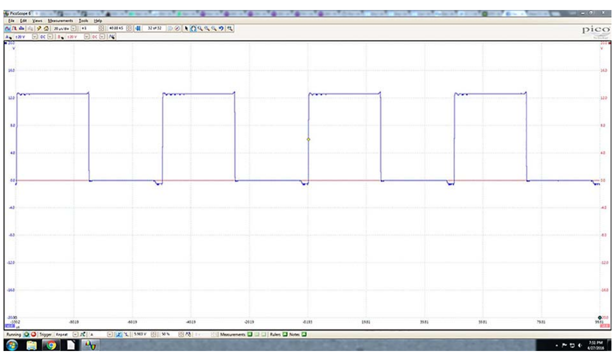

Fig. 12. Inverter output.

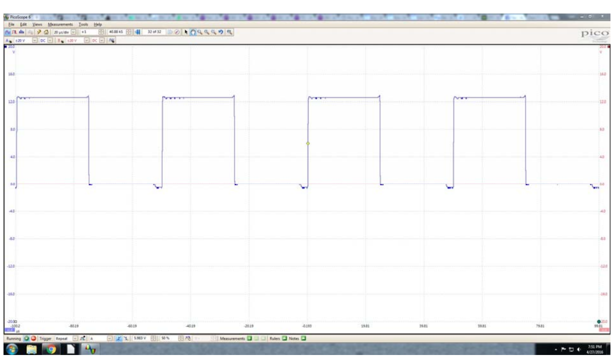

Fig. 13. Full h-bridge output, one inverter per channel

Following this, the coils were added in and the system was fully connected and powered. Fig. 14 shows the UWPT transmitting coil and receiving coil voltage at no load. During system testing it was discovered that there were high transient spikes caused by the sudden changes in current draw, and ugly ringing in the output signals shown in Fig. 15. This was fixed by adding a large capacitor to the input power rails, and smaller ones over the driver power input pins

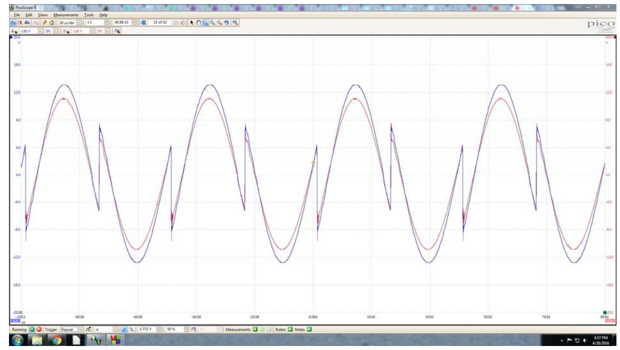

Fig.14. Tx and Rx coil voltage with no load.

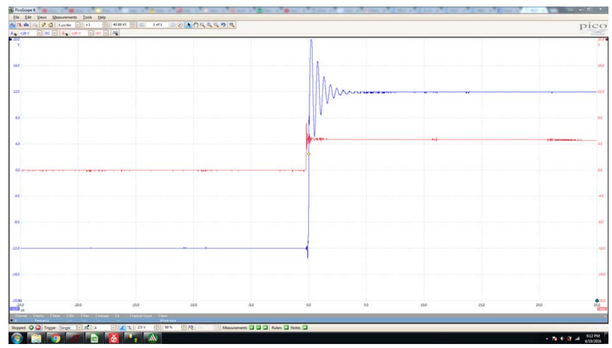

Fig. 15. High Transient.

A pair of drivers were killed by initiating the switching signals while the device was powered on. This can be prevented by applying power to the inverter while the ATmega328P is already providing the switching signals.

B. Full System Test

The full system was tuned to resonance with the Tx and Rx coils pressed right up against each other. With a load of 50Ω, the rectified VDC was 22.301V. This operating point of 9.94W was supplied by a battery charged to 13.5VDC, and at a frequency of 19.5kHz. Rectifier losses were estimated to be 0.223W, or 2.25% of received power.

VI. Conclusion

Wireless power transfer through resonant coupling was successfully achieved in an ocean simulated environment. Different configuration of coil design was analyzed and tested. While the transfer range was less than 10cm, there are several improvements to both system and coil design that can be made. Similarly, the implementation of a charging circuit can act as a load control if managed properly, further increasing overall efficiency. The results from the study is expected to provide guidelines to improve the efficiency and transmitting distance between the coils in underwater.

Future design improvements

The ocean environment is unstructured, uncertain and dynamic in nature. As a result, every system deployed into the harsh, complex environment encounters limitations. In the case of underwater wireless charging system, the physical limitations can include poor sensing capability. Looking ahead, we will evaluate the types of problems that may be created when power and data transfer are done simultaneously underwater. Also, the stochastic nature of the ocean environment will cause a frequent change in the coupling coefficient between the coils. Hence, an adaptive control that consider the dynamics of the coupling coefficient and still maintains maximum efficiency will be explored

Reference

[1] J. Shi, D. Li and C. J. Yang, "Design and analysis of an underwater inductive coupling power transfer system for autonomous underwater vehicle docking applications," *Journal of Zhejiang University SCIENCE C,* pp. 51-62, 9 January 2014.

[2] T. Orekan, P. Zhang, "Integrated dynamic modeling of a point absorber wave energy converter in regular and irregular waves," *in OCEANS 2015 - MTS/IEEE*, Washington, 2015.

[3] A. A. Han Jun, T. Ura, Y. Yagita and Y. Yamauchi, "High Speed Acoustic Network And Noncontact Power Supplier For Seafloor Geodetic Observing Robot System," in *IEEE*, Singapore, 2007.

[4] N. Shinohara, "Beam Control Technologies With a High-Efficiency Phased Array for Microwave Power Transmission in Japan," *Proceedings of the IEEE,* vol. 101, no. 6, pp. 1448 - 1463, 2013.

[5] S. G. Shan Jiang, "Electromagnetic Wave Propagation into Fresh Water," *Journal of Electromagnetic Analysis and Applications,* vol. 3, pp. 261-266, 2 June 2011.

[6] A. P. Sample, D. T. Meyer and J. R. Smith, "Analysis, Experimental Results, and Range Adaptation of Magnetically Coupled Resonators for Wireless Power Transfer," *IEEE Transactions on Industrial Electronics,* pp. 544-554, 22 March 2011.

[7] W. Fu, B. Zhang and D. Qiu, "Study on frequency-tracking wireless power transfer system by resonant coupling," in *Power Electronics and Motion Control Conference, 2009. IPEMC '09. IEEE 6th International*, Wuhan, 2009.

[8] H. Hwang, J. Moon, B. Lee, C.-h. Jeong and S.-w. Kim, "An Analysis of Magnetic Resonance Coupling Effects on Wireless Power Transfer by Coil Inductance and Placement," *IEEE Transactions on Consumer Electronics,* vol. 60, no. 2, pp. 203-209, 2014.